

pubs.acs.org/JPCB Article

Spectroelectrochemical and Computational Analysis of a Series of Cycloaddition—Retroelectrocyclization-Derived Donor—Acceptor Chromophores

Susannah D. Banziger,* Reese A. Clendening, Benjamin M. Oxley, and Tong Ren*



Cite This: J. Phys. Chem. B 2020, 124, 11901–11909



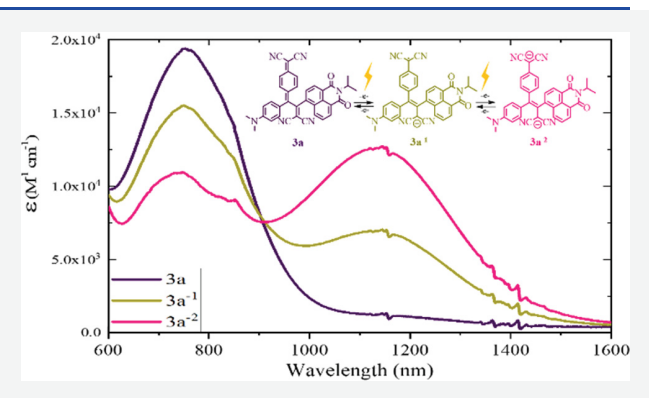
ACCESS

Metrics & More

Article Recommendations

s Supporting Information

ABSTRACT: The [2+2] cyclcoaddition (CA) and subsequent retroelectrocyclization (RE) reactions are useful in constructing nonplanar donor—acceptor chromophores that exhibit nonlinear optical properties and intramolecular charge-transfer transitions. However, both the infrared (IR) and visible—near IR (vis—NIR) spectroelectrochemical responses of CA-RE-derived chromophores are rarely explored in depth. Reported in this contribution is a comprehensive IR and vis—NIR spectroelectrochemical study of the CA-RE adducts of DMAP-C_{2n}-NAP^{iPr} of both tetracyanoethene (TCNE) and tetracyanoquinodimethane (TCNQ) and companion time-dependent density functional theory (TD-DFT) analysis of the bands observed. Specifically, DMAP-C_{2n}-NAP^{iPr} (1a, n = 1; 1b n = 2; DMAP = N_i N-dimethylaniline; NAP^{iPr} = N-isopropyl-1,8-naphthalimide) react with TCNE to yield the tetracyanobutadiene



(TCBD) derivatives (2a and 2b, respectively) and with TCNQ to yield the dicyanoquinodimethane (DCNQ) derivatives (3a and 3b, respectively). IR spectroelectrochemical studies showed the emergence/intensification of new CN stretches upon reductions. Ultraviolet−vis−NIR (UV−vis−NIR) spectroelectrochemical study of 3 revealed a partial bleach of the charge-transfer (CT) bands, originally appearing in the neutral species, and the emergence of new CT bands originating from NAP^{iPr} to the reduced DCNQ moiety. UV−vis−NIR spectroelectrochemical study of 2, surprisingly, indicated a very minimal change upon reductions. Dynamic changes were observed in the mid-IR absorption for C≡C and C≡N for both 2 and 3, indicative of enhanced asymmetry and the formation of ion pairs on the dicyano bridge. DFT and TD-DFT analyses were used to obtain the semi-quantitative pictures of the frontier orbitals of 1−3 and elucidate the origin of the transient features observed spectroelectrochemically for the 1e[−] and 2e[−] reduced species.

1. INTRODUCTION

A facile and useful reaction of acetylene-containing compounds is the [2+2] cycloaddition (CA) of electron-deficient olefin bonds, such as those in tetracyanoethene (TCNE) and tetracyanoquinodimethane (TCNQ), to the C≡C bond to form a cyclobutene ring and subsequent retroelectrocyclization (RE) to yield tetracyanobutadiene (TCBD, colored red in Scheme 1) and dicyanoquinodimethane (DCNQ, Scheme 1) functional groups, respectively. This type of reaction was first discovered by Bruce and co-workers with mononuclear Ru complexes and expanded to many metal alkynyl species in the ensuing decades.²⁻⁵ Because of its mild conditions and high yields, the cycloaddition-retroelectrocyclization (CA-RE) reaction has been adapted by materials chemists for the preparation of nonplanar push-pull chromophores.⁶⁻⁹ Among many interesting features revealed through the extensive studies of CA-RE derivatives are the rich redox characteristics: both TCBD and DCNQ groups often undergo two reversible one-electron reductions, rendering applications of CA-RE

Scheme 1. CA-RE Reactions to Yield TBCD and DCNQ

Received: October 19, 2020 Revised: December 4, 2020 Published: December 21, 2020



Scheme 2. D-B-A Dyads and Their CA-RE Adducts

derivatives as *p*-type dopants in organic electronics. Clearly, ultraviolet—visible (UV—vis) and infrared (IR) spectroscopic properties of these reduced species, both mono- and dianionic, are relevant to optoelectronic applications.

UV-vis and IR spectroelectrochemistry are important techniques for understanding mixed valency, 10,11 and recent years have seen many successful demonstrations in using spectroelectrochemistry to assess the degree of electronic delocalization in conjugated organometallic systems. 12-16 However, this powerful technique has rarely been applied to the CA-RE derivatives. Among a limited number of examples, Shoji et al. investigated the electrochromic behaviors of 2methyl-1-azulenyl-containing TCBD and DCNQ under stepwise reductions. Diederich and co-workers investigated the formation of CA-RE derivatives of DMAPC₄Fc (DMAP = N,N-dimethylaniline; Fc = ferrocenyl) of TCNE and TCNQ and recorded the UV-vis spectroelectrochemical behaviors of TCBD derivatives on both the oxidation of Fc and DMAP and the reductions of TCBD (Supporting Information). In a separate study, Diederich and co-workers reported the UV-vis spectroelectrochemical changes of a CA-RE derivative of 2,3,5,6-tetrafluoro-7,7,8,8-tetracyanoquinodimethane (F₄-TCNQ, spectra in the Supporting Information). 18 Misra and co-workers prepared both the TCBD and DCNQ derivatives of bisferrocene bridged by phenylacetylene and interrogated the changes of Vis spectra under the oxidation of Fc. 1

A recent focus of our laboratory is the understanding and attenuation of the photo-induced electron transfer process in a donor-bridge-acceptor (D-B-A) dyad, where the bridge can be either a conjugated organic fragment or metal alkynyl. 20,21 The compounds of particular interest to us are the dyads capped by N,N-dimethylaniline (DMAP, donor) and N-isopropyl-1,8-naphthalimide (NAPiPr, acceptor) with ethynyl (1a, Scheme 2) and butadiynyl (1b) bridges, which exhibit significant ground-state dipole moments and long-lived chargeseparated states upon electronic excitation.²¹ The use of NAP^{iPr} adds a robust chromophore for spectroscopic analysis as well as permanent polarity into the system of interest. In addition to the dynamics of photo-induced electron transfer, we are also intrigued about the prospect of 1a and 1b undergoing the CA-RE reaction and the electronic properties of the resultant derivatives (2 and 3 in Scheme 2). Described in this contribution are the synthesis and structural characterizations of compounds 2 and 3, spectroscopic and spectroelectrochemical studies of these compounds in both the neutral and multielectron reduced forms, and corroborative timedependent density functional theory (TD-DFT) analysis.

2. EXPERIMENTAL METHODS

2.1. Synthetic Details. All reactions were carried out using Schlenk techniques under N_2 . The preparation of N_1N_2 -dimethylaniline-4-ethynyl-4- N_2 -isopropyl-1,8-naphthalimide

(1a) was accomplished via the Sonogashira coupling of 4ethynyl-N,N-dimethylaniline and 4-bromo-N-isopropyl-1,8naphthalimide. Using a previously reported procedure, 2 was synthesized as a bright orange solid in 56% yield under weak base conditions in the presence of Pd(PPh₃)₂Cl₂ and CuI catalysts. N,N-dimethylaniline-4-butadiyne-4-N-isopropyl-1,8naphthalimide (1b) was obtained from the Cadiot-Chodkiewicz coupling reaction between 4-ethynyl-N,N-dimethylaniline and 4-bromo-4-ethynyl-N-isopropyl-1,8-naphthalimide (BrC2NAPiPr). Following the work of Gibtner et al., 23 a THF solution of BrC2NAPiPr was added dropwise to a pyridine/ THF solution containing CuI, nBuLi, and 4-ethynyl-N,Ndimethylaniline to yield 1b as a bright red solid in 51% yield. The TCBD (2a and 2b) and DCNQ (3a and 3b) derivatives of 1a and 1b were synthesized by the [2+2] CA-RE reaction. The reaction conditions were similar to those developed by Diederich and co-workers. The reaction of 1a in the presence of excess TCNE or TCNQ resulted in the formation of 2a (77% based on 1a) and 3a (39% based on 1a), respectively. Compounds **2b** (99% based on **1b**) and **3b** (39% based on **1b**) were formed similarly from 1b; however, the acetylene group adjacent to NAPiPr did not undergo cycloaddition due to its electron-poor nature. This is consistent with the CA-RE mechanism, in which insertion of TCNE or TCNQ to form TCBD or DCNQ, respectively, is initiated by an electron-rich alkyne. Similar reactivity was observed by Diederich and coworkers for dissymmetric butadiyne species and was exploited for regioselective addition of TCNE or TCNQ. 17 Compounds 2 and 3 were isolated as black crystalline solids. All compounds were characterized by UV-vis, Fourier transform infrared (FT-IR), and ¹H NMR spectroscopic techniques. Their electronic properties were probed experimentally with cyclic voltammetry (CV) and spectroelectrochemical techniques and analyzed with TD-DFT calculations. Additional experimental details can be found in the Supporting Information.

2.2. Instrumentation. UV-vis-NIR spectra were obtained with a JASCO V-780 UV-vis-NIR spectrophotometer. Infrared spectra were obtained on a JASCO FT-IR 6300 spectrometer via attenuated total reflectance (ATR) on a diamond crystal. ¹H NMR spectra were recorded on either a Varian MERCURY300 or a Varian Inova300 NMR spectrometer. Cyclic voltammograms were recorded in 0.1 M n-Bu₄NPF₆ and 1.0 mM analyte solution (CH₂Cl₂, Ar degassed) using a CHI620A voltammetric analyzer with a glassy carbon working electrode (diameter = 2 mm), Pt-wire counter electrode, and an Ag/AgCl reference electrode with ferrocene used as an external reference (Figure S1). Spectroelectrochemical absorption data was taken with a JASCO V-780 UV-vis-NIR spectrophotometer, and IR data was taken on a JASCO FT-IR 6300 spectrometer. Spectroelectrochemical analysis was performed using an optically transparent thin-layer electrochemistry (OTTLE) liquid-sample cell²⁴ with a 0.2 mm optical path length, 0.3 mL sample volume, and a CaF₂ window. The cell was equipped with a mesh Pt working electrode, mesh Pt auxiliary electrode, and Ag reference electrode; the analyte concentration was 2–5.0 mM in 4 mL of dry dichloromethane at a 0.1 M Bu₄NPF₆ electrolyte concentration. X-ray diffraction (XRD) data (Tables S1 and S2) for 1b was obtained on a Bruker Quest diffractometer with MoK α radiation (λ = 0.71073 Å) at 150 K. XRD data for 1a, 2a, and 3b were obtained on a Bruker Quest diffractometer with CuK α radiation (λ = 1.54178 Å) at 150 K.

2.3. Computational Details. DFT and TD-DFT calculations for compounds 1–3 were performed using the MN15 functional²⁵ and the Def2-SVP basis set²⁶ as implemented in Gaussian 16.²⁷ The calculated spectra provided by the MN15 functional were in good agreement with the experimentally observed FT-IR and UV-vis-NIR spectra. The CAM-B3LYP functional²⁸ was also tested and showed similar results. Also tested was the B3LYP density functional theory^{29,30} and the 6-31G (d,p) basis set,³¹ which provided a poor fit for the reduced complexes. The polarizable continuum model (PCM)³² was used to simulate the solvent effects of dichloromethane in both the neutral and anionic state calculations. Coordinates of the optimized geometries in the ground state are listed in Table S3.

3. RESULTS AND DISCUSSION

3.1. Syntheses. Compounds 1a (*N*,*N*-dimethylaniline-4-ethynyl-4-*N*-isopropyl-1,8-naphthalimide) and 1b (*N*,*N*-dimethylaniline-4-butadiyne-4-*N*-isopropyl-1,8-naphthalimide)²¹ were prepared from Sonogashira and Cadiot—Chodkiewicz coupling reactions, respectively, and the details are reported in the Supporting Information. The CA-RE reactions of 1 with TCNE proceeds at ambient conditions in very good yields of 2, while those with TCNQ requires extensive heating, and the isolated yields of 3 are modest (see the Supporting Information for preparation and purification details).

3.2. Structural Analysis. Single crystals of **1a** (Figure 1) and **1b** (Figure 2) were grown from slow diffusion of hexanes

Figure 1. ORTEP plot of **1a** at 30% probability level; hydrogen atoms and disorder were omitted for clarity. Selected bond lengths (Å): C1–C2 1.205 (2), C2–C3 1.401 (4), C1–C18 1.431 (2).

Figure 2. ORTEP plot of **1b** at 30% probability level; hydrogen atoms and disorder were omitted for clarity. Selected bond lengths (Å): C1–C2 1.210 (4), C3–C4 1.211 (5), C1–C3 1.364 (4), C2–C5 1.425 (4), C4–C20 1.420 (5).

into CH₂Cl₂. Crystals of compound 2a (Figure 3) were grown via slow evaporation of a concentrated solution of hexanes/

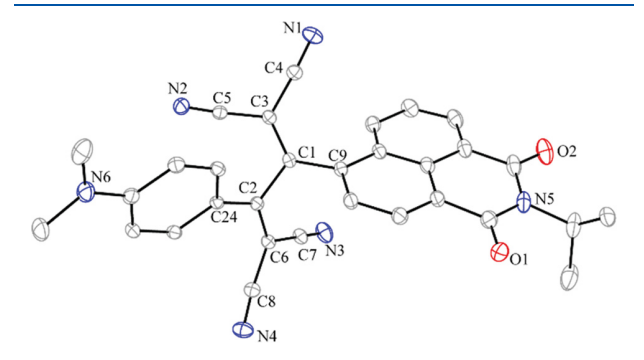


Figure 3. ORTEP plot of **2a** at 30% probability level; hydrogen atoms and disorder were omitted for clarity. Selected bond lengths (Å): C1–C2 1.502 (2), C1–C9 1.482 (3), C2–C24 1.441(2), C4–N1 1.146 (2), C5–N2 1.145 (2), C7–N3 1.148 (2), C8–N4 1.145 (2).

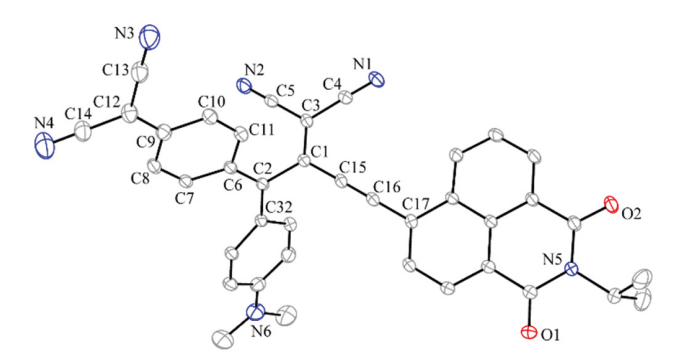


Figure 4. ORTEP plot of **3b** at 30% probability level; hydrogen atoms and disorder were omitted for clarity. Selected bond lengths (Å): C1–C2 1.503 (3), C15–C16 1.197 (3), C4–N1 1.145 (3), C5–N2 1.151 (3), C13–N3 1.148 (4), C14–N4 1.150 (4).

EtOAc (3:1), while those of compound 3b (Figure 4) were grown via slow diffusion of hexanes into chloroform. An extended table of bond lengths and angles as well as experimental crystal data is provided in Tables S1 and S2. The C≡C bond lengths were within the expected range, as were the C≡N bond lengths. Comparison of the C1-C2 bond lengths of 1a and 2a confirms the conversion of the C≡ C triple bond in 1a (1.205 (2) Å) to a single bond in 2a (1.502 A)(2) Å) upon the CA-RE reaction. The dihedral angle around the central C-C bond of 2a (C3-C1-C2-C6) is 125.3 (1)° with the dicyanomethine moieties anti to each other, and the C3-C1-C2 and C1-C2-C6 bond angles are 118.9 (1)° and 116.9 (1)°, respectively. Compound 3b adopts a similar conformation, with the dicyanoquinone insertion taking place adjacent to DMAP. Notably, only one TCNQ insertion occurs, with the C≡C bond adjacent to NAPiPr (C15-C16 1.197 (3) Å) remaining intact.

3.3. Electrochemistry. Compounds 1 display two one-electron processes in their cyclic voltammograms: a reversible reduction localized on NAP^{iPr} and an irreversible oxidation localized on DMAP. The irreversible nature of the latter is attributed to the chemical instability of an *N*-based radical cation. Compared to 1a, electrode potentials for 1b are anodically shifted by 50 mV (oxidation) and 110 mV

(reduction), reflecting the increased electron deficiency of butadiyne from ethyne. The electrochemical highest occupied molecular orbital–lowest occupied molecular orbital (HOMO–LUMO) gap ($E_{\rm g}=E_{\rm pa}(+1/0)-E_{\rm pa}(0/-1))$ was calculated and listed, along with the optical HOMO–LUMO gap ($E_{\rm op}/{\rm eV}=10^7/8065.5\lambda_{\rm max}$). It is clear that the $E_{\rm g}$ and $E_{\rm op}$ display the same trend, that is, 1 > 2 > 3, while the latter is ca. 0.6 eV larger than the former. This is consistent with the simple relationship suggested by Loutfys: $E_{\rm op}=E_{\rm g}+(2K-J)$, where K and J are the Coulomb and exchange integrals, respectively. 33

The CVs of the TCNE CA-RE adducts, compounds 2, feature prominently a pair of reversible one-electron reductions attributed to the TCBD group, and the added electrons are presumably delocalized over the entire TCBD moiety with $\Delta E_{1/2}$ values of 430 and 380 mV for 2a and 2b, respectively. The insertion increases the electron deficiency greatly, as evidenced by a ca. 400 mV shift in E(+1/0). Interestingly, the heightened electron deficiency also stabilized the N-based radical cation and renders the oxidation reversible. Furthermore, $E_{1/2}(+1/0)$ s for 2a and 2b are identical within experimental errors, indicating electronic decoupling between the DMAP and NAP^{iPr} groups. Upon insertion, the reduction couples of NAP^{iPr} are cathodically shifted by 340 and 240 mV in 2a and 2b, respectively. The cause of large shifts is electrostatic: the electroactive species is already dianionic and hence harder to reduce further. The proximity of NAP^{iPr} to TCBD in 2a results in a larger shift than in 2b.

The insertion of TCNQ seems less impactful on the voltammetric characteristics than that of TCNE. The $E_{\rm pa}(+1/0)$ s for both ${\bf 3a}$ and ${\bf 3b}$ remain the same as those for ${\bf 1a}$ and ${\bf 1b}$, respectively, and the couples are irreversible, indicating a minimum interaction between the DMAP and DCNQ groups. The reduction couples of NAP^{iPr} in ${\bf 3a}$ and ${\bf 3b}$ are cathodically shifted but of smaller magnitude compared to those of ${\bf 2a}$ and ${\bf 2b}$, and the shift is similarly attributed to the electrostatic effect. Two reversible one-electron reductions attributed to DCNQ are separated by 200 and 170 mV for ${\bf 3a}$ and ${\bf 3b}$, respectively. These results are shown in Figure 5 and summarized in Table 1.

3.4. UV-vis Absorption Spectroscopy. The electronic absorption spectra of compounds 1, 2, and 3 are shown in Figure 6. The spectra of linear D-B-A compounds 1a and 1b (Figure 6a) consist of two main peaks. The higher energy peaks at 315 nm (1a) and 338 nm (1b) are assigned to the $\pi(DMAP) - \pi^*(DMAP-NAP^{iPr})$ transition (Figure S2). Given that HC₂DMAP absorbs at 290 nm, it is likely that this transition is highly influenced by the donor.³⁴ The visible peaks at 455 nm (1a) and 453 nm (1b) are attributed to the CT transition $\pi(DMAP) - \pi^*(NAP^{iPr})$ as corroborated by TD-DFT (Figure S3). The $\pi-\pi^*$ transition localized on NAP^{iPr} (350 nm in HC₂NAP^{iPr})³⁴ is weak in **1b** (shoulders at ca. 375 nm) and absent in 1a. The TCBD derivatives 2a and 2b display a new intense peak in the visible region (540 nm in 2a and 550 nm in 2b). The appearance of such peaks has been observed for related TCBD species, 35,36 and similar peaks are generally assigned as the donor to $\pi^*(TCBD)$ transitions. In the case of 2a and 2b, the absorptions are largely attributed to the $\pi(DMAP)-\pi^*(TCBD)$ transition based on TD-DFT analysis (see discussion below). The DCNQ derivatives 3a and 3b are deeply colored, and correspondingly, their absorption spectra feature a very intense peak in the red region (748/741 nm for 3a/3b), which is attributed to the

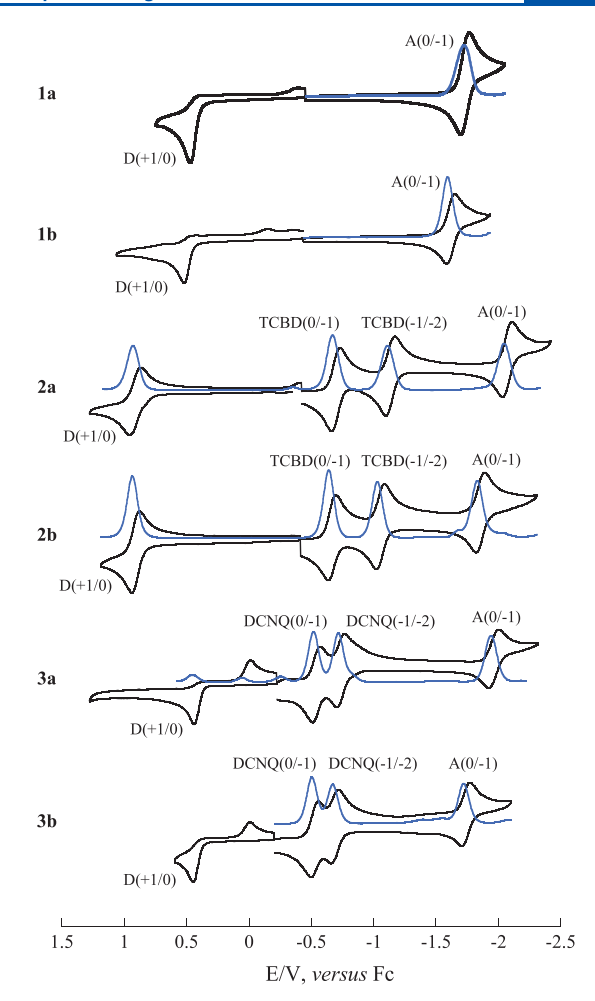


Figure 5. Cyclic (black) and differential pulse (blue) voltammograms of compounds 1-3 in dichloromethane, 1 mM analyte with 0.1 M nBu_4PF_6 . $A=NAP^{iPr}$; D=DMAP.

Table 1. Electrochemical Potentials (V) in Dichloromethane, 1 mM Analyte with 0.1 M n-Bu₄NPF₆^a

	$E(+1/0) \atop (\Delta E_{\text{p}; i_{\text{b}}} i_{\text{b}} / i_{\text{f}})$	$E(0/-1)$ (TCBD/DCNQ) $(\Delta E_{p_i} i_b/i_f)$	$\begin{array}{c} E(-1/-2) \\ (\text{TCBD/} \\ \text{DCNQ}) \\ (\Delta E_{\text{p}i} i_{\text{b}} / \\ i_{\text{f}})^{b} \end{array}$	$\begin{array}{c} \mathbf{E(NAP)} \\ (\Delta E_{\mathbf{p}_{1}^{*}} i_{\mathbf{b}} / \\ i_{\mathbf{f}}) \end{array}$	$E_{ m g}$ /V	$\frac{E_{\mathrm{op}}}{(v/\mathrm{cm}^{-1})}$
1a	0.47 ^b			-1.73 (0.068)	2.20	2.74 (22,100)
1b	0.52 ^b			-1.62 (0.066)	2.14	2.73 (22,000)
2a	0.91 (0.09)	-0.70 (0.069)	-1.13 (0.072)	-2.07 (0.076)	1.61	2.23 (18,000)
2b	0.91 (0.062)	-0.67 (0.061)	-1.05 (0.066)	-1.86 (0.069)	1.58	2.25 (18,100)
3a	0.44 ^b	-0.54 (0.061)	-0.74 (0.062)	-1.96 (0.081)	0.98	1.65 (13,300)
3b	0.45 ^b	-0.52 (0.062)	-0.69 (0.06)	-1.74 (0.064)	0.97	1.68 (13,600)

^aElectrode potentials vs Fc⁺/Fc with peak separation $(\Delta E_{\rm p})$ for reversible processes shown in parentheses. ^bIrreversible redox events. The CV of the Fc standard is displayed in Figure S1.

 $\pi(\text{DMAP}) - \pi^*(\text{DCNQ})$ transition (Figure S3). The enhanced intensity reflects the fact that the DCNQ group is a far more effective acceptor than the TCBD group.

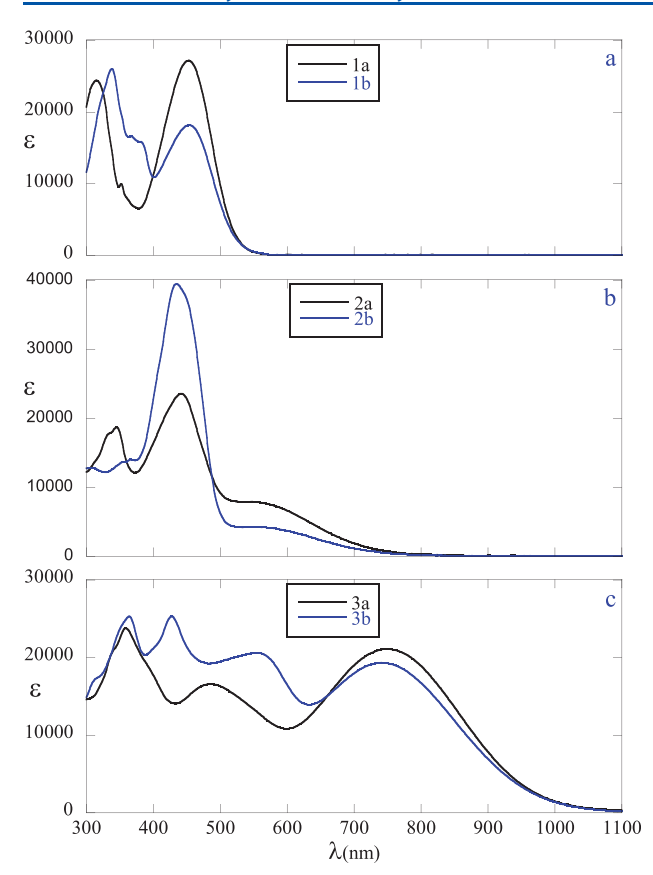


Figure 6. UV-vis absorption spectra of (a) 1a/1b; (b) 2a/2b; and (c) 3a/3b in CH₂Cl₂.

3.5. FT-IR Spectroelectrochemistry. Compounds 1, 2, and 3 exhibit peaks associated with both C≡C and C≡N stretches in the window of 2100-2300 cm⁻¹ that is free of any other peaks. Changes in this region upon sequential oneelectron reductions may reveal intimate details of transformations in the electronic structures. Peak assignment of the observed triple bond stretches was achieved through a direct comparison of the stretching frequencies of 2a (Figure 7) to 2b (Figure S4) and 3a (Figure 8) to 3b (Figure S5). Compound 2a has a unique C≡N stretch at 2209 cm⁻¹; therefore, the C≡N stretch in 2b can be assigned to the higher energy peak also at 2214 cm⁻¹, and the C≡C stretch can be assigned to the lower energy stretch at 2180 cm⁻¹. Similarly, 3a has a strong C≡N stretch at 2203 cm⁻¹, and 3b has a strong C \equiv N stretch (2201 cm $^{-1}$) and a lower frequency C \equiv C stretch $(2174 \text{ cm}^{-1}).$

Upon the reduction of compounds 2 or 3, $\nu(C \equiv N)$ was greatly affected, suggesting that the reductions are occurring at the TCDB or DCNQ bridge, respectively. Based on literature precedence, the first reduction took place at the dicyanomethine group adjacent to the acceptor (NAP^{iPr}), as shown in Chart 1.^{37–39} For both 2a (Figure 7) and 2b (Figure S4), an intense peak at 2146 cm⁻¹ arises for the TCBD⁻¹ species (red line), which is attributed to an enhanced asymmetry in the bridge. Further reduction results in the formation of TCBD⁻², which is characterized by the decay of a peak at 2146 cm⁻¹ and the growth of a peak at ~2185 cm⁻¹. This peak is partially masked in 2b due to the presence of the C \equiv C stretch (Figure S4). ^{17,31}

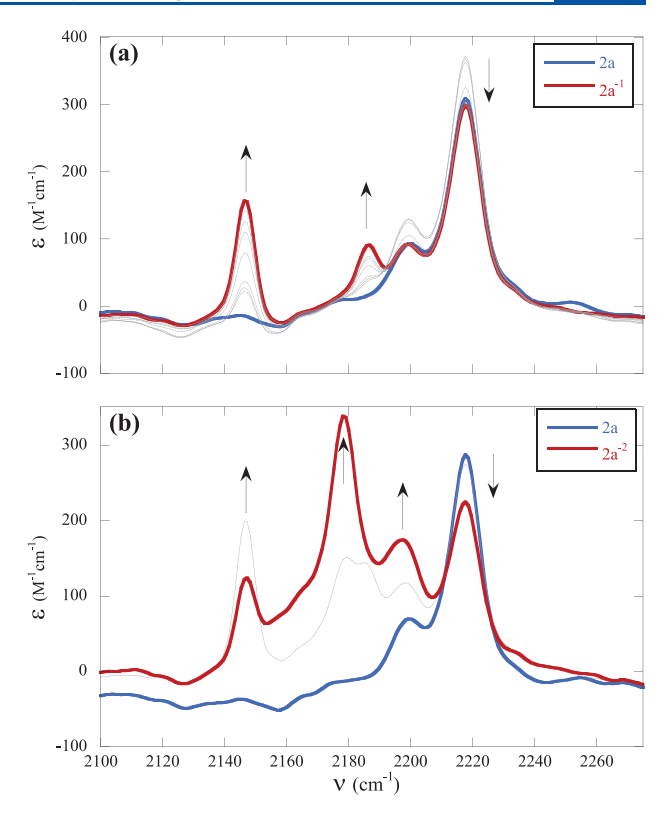


Figure 7. FT-IR spectroelectrochemical changes for 2a upon the first reduction at -0.25 V (a) and second reduction at -0.70 V (b) in CH₂Cl₂, 5 mM analyte with 0.1 M Bu₄NPF₆.

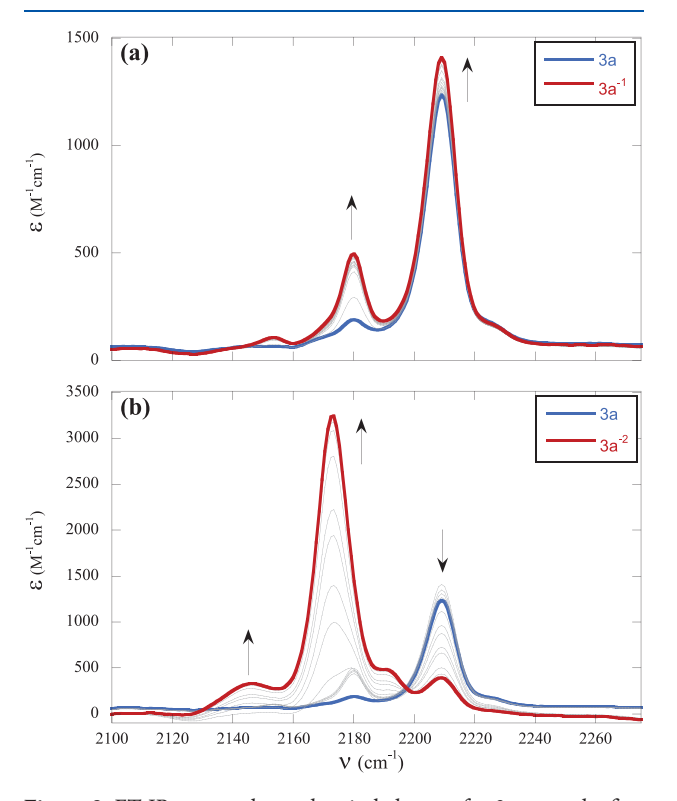


Figure 8. FT-IR spectroelectrochemical changes for 3a upon the first reduction at $-0.15~\rm V$ (a) and second reduction at $-0.50~\rm V$ (b) in $CH_2Cl_2,~4~\rm mM$ analyte with 0.1 M $Bu_4NPF_6.$

Chart 1. Predicted Electrochemical Reduction Products for the First and Second Reduction, Where m = 0 (2a) or 1 (2b)

The $\nu(C\equiv N)$ changes observed for compound 3a, IR shown in Figure 8, follow the predicted trend for the reduction of TCNQ, ⁴⁰ in which a new C \equiv N stretch grows in at a lower frequency (compared to the neutral species) for $3a^{-1}$ (2180 cm⁻¹) and an even lower energy peak grows in for TCNQ⁻² (2145 cm⁻¹). The reduction of 2 and 3, resulting in lower $\nu(C\equiv N)$ stretches, is consistent with the weakening of the C \equiv N bond due to the reduced π -bond order ⁴¹ and could indicate a ketenimine resonance structure to stabilize the negative charge (Chart 2). ⁴² Other literature examples suggest

Chart 2. Ketenimine Anion Resonance Structure

that the increased number of $C \equiv N$ stretching frequencies is attributed to the reduced symmetry from the formation of ion pairs on the dicyano bridge.^{43,44}

3.6. UV–vis Spectroelectrochemistry. The TCBD species exhibited a hypsochromic shift of the $\lambda_{\rm max}$ after the first reduction and a bathochromic shift of the $\nu_{\rm max}$ upon further reduction (Figure 9 and Figure S6). Comparatively, the

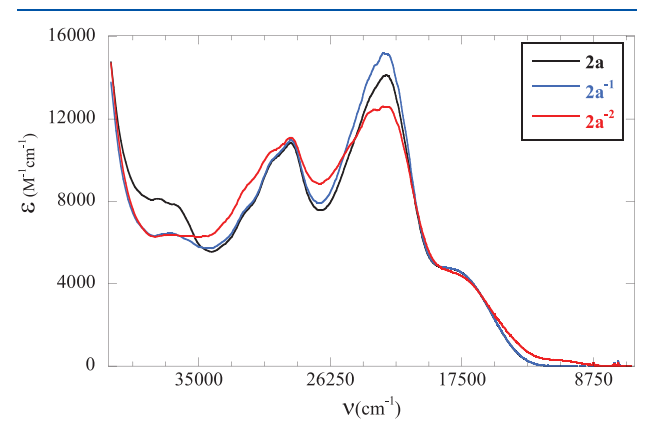


Figure 9. UV–vis spectroelectrochemical changes for 2a upon the first reduction at -0.25 V (blue) and second reduction at -0.70 V (red) in CH_2Cl_2 , 5 mM analyte with 0.1 M Bu_4NPF_6 .

DCNQ compounds underwent a bathochromic shift of the $\nu_{\rm max}$ upon the first reduction. When reduced further to the dianionic species, the extinction coefficients for the new peak increases for 3a but decreases for 3b. These spectral changes were ascribed to the mono- and dianion, respectively, (Figure 10 and Figure S7). The uncharged species for 2a, 2b, and 3a could be recovered upon oxidation, and their calculated band gaps are given in Figure 11.

Spectral changes observed for 2a and 2b upon reduction are shown in Figure 9 and Figure S6, respectively. Upon the first

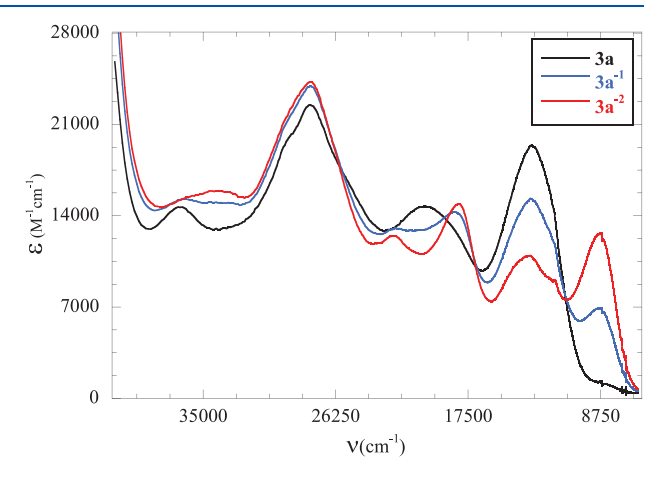


Figure 10. UV–vis spectroelectrochemical changes for 3a upon the first reduction at -0.15 V (blue) and second reduction at -0.50 V (red) in CH_2Cl_2 , 2 mM analyte with 0.1 M Bu_4NPF_6 .

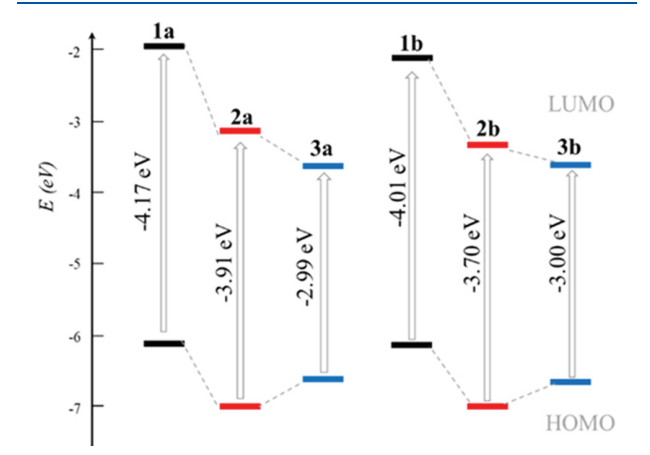


Figure 11. Energy diagrams and subsequent band gaps for compounds 1, 2, and 3 estimated from DFT calculations.

reduction of the TCBD species (2a and 2b), there is a significant decrease in intensity at ~38,000 cm⁻¹ and a minimal change for the intramolecular CT band at ~17,500 cm⁻¹. A similar trend was observed in the spectroelectrochemical study of dissymmetric TCBD species substituted with an azulene ring by Shoji.³⁸ Upon the second reduction, a new but weak transition grows in between 11,000 and 10,000 cm⁻¹ for both 2a and 2b. TD-DFT analysis of the doubly reduced form of 2 (Figure 12) suggests that this transition can be assigned to $\pi(\text{NAP}) \to \pi^*(\text{DMAP-NAP}^{i\text{Pr}})$ for $2a^{-2}$ and $\pi(\text{NAP}) \to \pi^*$ of the electron-deficient bridging carbons in TCBD for $2b^{-2}$. The most intense peak at 22,000 cm⁻¹, assigned primarily to $\pi(NAP) \rightarrow \pi^*(TCBD)$ (Figure S8), intensifies on the first reduction and decays significantly on the second reduction. TD-DFT analysis of 2a suggests that the increase in intensity is due to the increased electron density on the bridging TCBD,

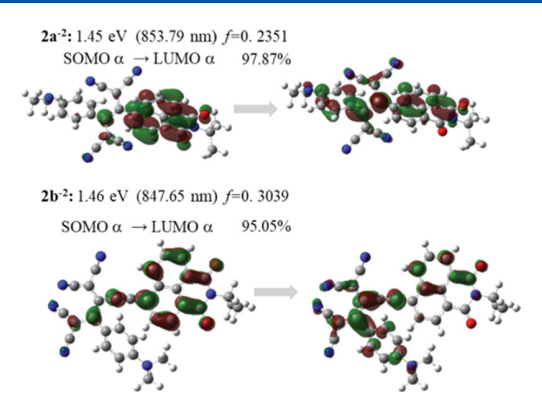


Figure 12. TD-DFT results showing the major orbital transitions that contribute to the lowest energy transition observed in the UV-vis region for $2a^{-2}$ versus $2b^{-2}$.

and the subsequently decreased intensity is a result of the transition being shifted to a higher energy (Figure S9). In comparison, the TCBD derivative of DMAPC₄Fc displays a new low energy band (ca. 700 nm) with a concurrent decay of the original CT band (ca. 530 nm) on the first reduction, and both bands disappear upon the second reduction.¹⁷ While the strong absorption from NAPiPr masks the spectral changes between 300 and 600 nm, compound 2b undergoes a similar process to that of the TCBD derivative of DMAPC₄Fc upon reduction to $2b^{-2}$ (Figure S6). The appearance of a low energy band on the second reduction instead of the first is most likely due to the electron-deficient nature of NAPiPr, causing the (TCBD)⁻¹ moiety to act as a donor, with the lowest energy transition assigned as $\pi(TCBD) \rightarrow \pi^*(NAP^{iPr})$ (Figures S10 and S11). Reduction to the dianion localizes the electron density on the cyano groups of TCBD and compels NAP^{iPr} to behave as a surrogate donor to the electron-deficient bridging carbons, labeled as 1 and 2 in Chart 1. This gives rise to a lower energy transition originating from $\pi(NAP)$ (as noted above), which is assigned to the experimentally observed transition between 10,000 and 11,000 cm⁻¹ upon the second reduction. Compared to $2b^{-2}$, $2a^{-2}$ exhibits more diffuse electron delocalization across the whole complex (Figure 12).

The spectroelectrochemical responses of DCNQ-type compounds, 3a (Figure 10) and 3b (Figure S7), are more dynamic compared to those of 2a and 2b. The reduction of 3a to $3a^{-1}$ resulted in the growth of a new band at 8700 cm⁻¹ (6800 M⁻¹ cm⁻¹). The extinction coefficient of this transition was nearly doubled (12,800 M⁻¹ cm⁻¹) upon further reduction to $3a^{-2}$, and the solution turned from dark purple to bright pink. This drastic change can be attributed to the increased aromaticity within the DCNQ group. Unlike complexes 2a and 2b, TD-DFT analysis of $3a^{-2}$ (Figure 13 and Figure S12) indicated that the lowest energy transition was primarily attributed to $\pi(NAP^{iPr}) \to \pi^*(NAP^{iPr})$ with some contribution from $\pi(DCNQ) \rightarrow \pi^*(NAP^{iPr})$, which intensifies with the increased electron density on the DCNQ group. The spectral evolution of 3b upon reduction follows a trend parallel to that of 3a. However, the transition observed at ~9000 cm⁻¹ was significantly weaker $(3b^{-1}, 3000 \text{ M}^{-1} \text{ cm}^{-1}; 3b^{-2}, 1000 \text{ M}^{-1} \text{ cm}^{-1})$ since the C=C spacer significantly dampens the conjugation between DCNQ and NAPiPr (Figure S13). Unlike the cases of 2a/b and 3a, the original spectrum of 3b could not be recovered upon re-oxidation. This poor spectroscopic reversibility has been observed in the DCNQ species studied

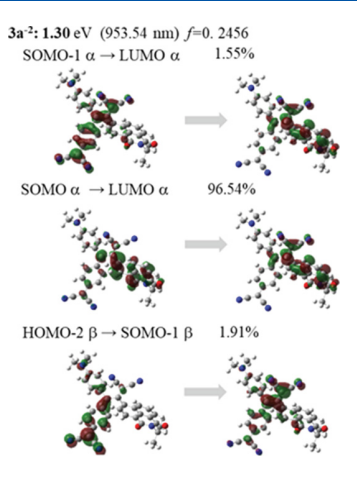


Figure 13. TD-DFT results showing the major orbital transitions that contribute to the lowest energy transition observed in the UV-vis for compound $3a^{-2}$.

by Shoji and co-workers, who assigned this behavior to the formation of a σ -bonded DCNQ dimer from the radical anions generated upon the first reduction. ^{18,38}

3.7. DFT Analysis. The optimized structures were used for the ground states of 1-3 and the reduced forms of 2 and 3 for the DFT and TD-DFT calculations. The computed energy levels for the frontier orbitals are shown in Figure 11, revealing a trend of HOMO-LUMO gaps consistent with the E_{op} for the lowest energy peaks observed. TD-DFT analysis (Figure S3) suggests that the bands at ~455 nm for 1a and 1b correspond to the DMAP (HOMO) to NAP^{iPr} (LUMO) transitions. The new CT transitions at ~545 nm in compounds **2a** and **2b** are mostly attributed to $\pi(DMAP) - \pi^*(TCBD)$. Furthermore, there is a marked difference in the ε at \sim 440 nm between 2a (442 nm (23,600 cm⁻¹ M⁻¹)) and 2b (435 nm (39,500 cm⁻¹ M⁻¹)). This can be attributed to the increased conjugation resulting from the C≡C bond in series 2b and is reflected in a higher calculated frequency for 2b (Figure S8).³¹ Introduction of DCNQ results in an even lower energy intramolecular CT band at \sim 745 nm with comparable ε for 3a and 3b and is primarily assigned to the interaction between DMAP and the DCNQ moiety (Figure S3). Furthermore, 3a (DCNQ) exhibits significantly stronger solvatochromism of the intramolecular CT band compared to 2a (TCBD). Normalized absorption data (Figure S14) shows a shift of approximately 50-100 nm for 3a, compared to a ~20 nm shift for 2a in solutions of EtOAc ($\varepsilon = 6$), CH₂Cl₂ ($\varepsilon = 9$), and CH₃CN (ε = 37). This trend was observed by Diederich for DCNQ species and was attributed primarily to solvent polarizability and cavity size.⁴⁵

TD-DFT analysis provided further understanding of the nature of the transitions observed in the UV-vis-NIR spectroelectrochemistry study. Both the major orbital contributions and oscillator strengths for the lowest energy transitions for 1a-3a are summarized in Table 2 and for 1b-3b in Table S4, and the corresponding orbitals involved are shown in the Supporting Information. These calculations indicated that the lowest energy transitions are generally CT bands from a donor to an acceptor.

As discussed previously, the reduction of compounds 2 and 3 resulted in significant changes in the UV-NIR-IR spectra, and changes in 3 are more drastic than those in 2. The first and second reductions of these compounds occur at the TCBD and

Table 2. Results of the TD-DFT Calculations of the Electronic Absorption Spectrum for Series "a" Showing the Major Transitions for the Lowest Energy Absorption Band. Calculated Wavelength ($\lambda_{\rm calc}$) Is Reported in nm and Wavenumber (ν) Is Reported in cm⁻¹

	$\lambda_{\rm calc} \ (v)$	oscillator strength	major contributions
1a	438 (22,830)	1.0643	$\text{H-1} \rightarrow \text{LUMO (4.18\%)}\text{HOMO} \rightarrow \text{LUMO (92.83\%)}$
2a	527 (18,980)	0.1873	$HOMO \rightarrow LUMO (96.90\%)$
$2a^{-1}$	781 (12,800)	0.0648	SOMO \rightarrow LUMO (96.45%)SOMO \rightarrow L + 1 (3.55%)
$2a^{-2}$	854 (11,710)	0.2351	SOMO \rightarrow LUMO (97.87%)SOMO \rightarrow L + 2 (2.13%)
3a	679 (14,730)	0.6702	HOMO → LUMO (98.61%)
3a ⁻¹	1026 (9750)	0.3897	SOMO → LUMO (1.29%)SOMO → L + 1 (2.16%)H-2 → SOMO (1.39%)H- 1 → SOMO (95.19%)
$3a^{-2}$	954 (10,480)	0.2456	S-1 → LUMO (1.55%)SOMO → LUMO (96.54%)H-2 → S-1 (1.91%)

DCNQ groups, making these functional groups more electron-donating than electron-withdrawing. Figures 12 and 13 show the orbitals involved in the lowest energy transition for $2a^{-2}$ and $3a^{-2}$, which can be assigned to $\pi(\text{NAP}^{iPr}) \to \pi^*(\text{DMAP-NAP}^{iPr})$ and $\pi(\text{NAP}^{iPr}) \to \pi^*(\text{NAP}^{iPr})$, respectively.

4. CONCLUSIONS

Reported herein is a comprehensive study of the electrochromic behavior of TCBDs (2a and 2b) and DCNQs (3a and 3b) and the respective energetic assignments based on TD-DFT analyses. Drastic changes in the IR spectra were observed for the reduced forms of the TCBDs and DCNQs, which are consistent with the theoretical models of the reduced forms of TCNQ⁴⁰ and the experimental data of the reduced forms of TCNE and TCNQ. To our knowledge, this is the first example of IR spectroelectrochemical studies of organic TCBD and DCNQ compounds.

TD-DFT was employed to better understand the transitions observed for the reduced forms of 2 and 3 in the electronic absorption spectra. Each subsequent reduction increases the electron density on the TCBD or DCNQ moiety, shifting the CT bands to lower energies. Notably, the reduced forms of compound 3a had a strong absorption at ca. 9000 cm⁻¹, which was attributed to an increased conjugation within the molecule.

These results suggest that the TCNE or TNCQ insertion into a dissymmetric donor—acceptor dyad has a profound effect on the identity and energetics of the CT band observed in the UV—vis—NIR region. Furthermore, the presence of a C≡C spacer (2b and 3b) seems to have little effect on the spectroelectrochemical changes observed for the TCBD series yet significantly decreases the strength of the CT band observed for the reduced forms of 3b relative to those of 3a. Work is currently underway furthering this class of compounds with efforts focused on altering the donor and the alkynyl bridge length.

ASSOCIATED CONTENT

Supporting Information

The Supporting Information is available free of charge at https://pubs.acs.org/doi/10.1021/acs.jpcb.0c09450.

1a sc980b final (CIF)

Additional FT-IR and UV—vis spectroelectrochemistry data, crystallographic information for compounds 1a, 1b, 2a, and 3b, and extensive tabulation of TD-DFT analysis (PDF)

AUTHOR INFORMATION

Corresponding Authors

Susannah D. Banziger — Department of Chemistry, Purdue University, West Lafayette, Indiana 47907, United States; Email: cox55@purdue.edu

Tong Ren – Department of Chemistry, Purdue University, West Lafayette, Indiana 47907, United States; ⊙ orcid.org/ 0000-0002-1148-0746; Email: tren@purdue.edu

Authors

Reese A. Clendening — Department of Chemistry, Purdue University, West Lafayette, Indiana 47907, United States Benjamin M. Oxley — Department of Chemistry, Purdue University, West Lafayette, Indiana 47907, United States

Complete contact information is available at: https://pubs.acs.org/10.1021/acs.jpcb.0c09450

Notes

The authors declare no competing financial interest.

ACKNOWLEDGMENTS

We gratefully acknowledge financial support from the National Science Foundation (CHE 1764347 and CHE 1625543). S.D.B. and R.A.C. thank Purdue University for a *Cagiantas Fellowship* and a *Ross Fellowship*, respectively. We thank Dr. Brandon L. Mash for assistance with X-ray data collection of 1b and Dr. Adharsh Raghavan for sharing his computational expertise.

REFERENCES

- (1) Bruce, M. I.; Rodgers, J. R.; Snow, M. R.; Swincer, A. G. Cyclopentadienyl-Ruthenium and Cyclopentadienyl-Osmium Chemistry Cleavage of Tetracyanoethylene under Mild Conditions X-Ray Crystal-Structures of Ru(Eta-3-C(Cn)2cphc=C(Cn)2)(Pph3)-(Eta-C5h5) and Ru(C =C(Cn)2 Cph=C(Cn)2)-(Cnbut)(Pph3)-(Eta-C5h5). J. Chem. Soc., Chem. Commun. 1981, 271–272.
- (2) Bruce, M. I. Some Organometallic Chemistry of Tetracyanoethene: CN-displacement and Cycloaddition Reactions with Alkynyl-Transition Metal Complexes and Related Chemistry. *Aust. J. Chem.* **2011**, *64*, 77–103.
- (3) Bruce, M. I. Reactions of polycyano-alkenes with alkynyl- and poly-ynyl-Group 8 metal complexes. *J. Orgnomet. Chem.* **2013**, 730, 3–19.
- (4) Xi, B.; Liu, I. P. C.; Xu, G.-L.; Choudhuri, M. M. R.; DeRosa, M. C.; Crutchley, R. J.; Ren, T. Modulation of Electronic Couplings within Metal-Polyyne Frameworks. *J. Am. Chem. Soc.* **2011**, *133*, 15094–15104.
- (5) Pigulski, B.; Gulia, N.; Szafert, S. Reactivity of Polyynes: Complex Molecules from Simple Carbon Rods. *Eur. J. Org. Chem.* **2019**, 1420–1445.
- (6) Wu, X.; Wu, J.; Liu, Y.; Jen, A. K.-Y. Highly efficient, thermally and chemically stable second order nonlinear optical chromophores containing a 2-phenyl-tetracyanobutadienyl acceptor. *J. Am. Chem. Soc.* 1999, 121, 472–473.
- (7) Kato, S.-i.; Diederich, F. Non-planar push-pull chromophores. *Chem. Commun.* **2010**, 46, 1994–2006.

- (8) Bures, F. Fundamental aspects of property tuning in push-pull molecules. RSC Adv. 2014, 4, 58826–58851.
- (9) Kivala, M.; Diederich, F. Acetylene-Derived Strong Organic Acceptors for Planar and Nonplanar Push-Pull Chromophores. *Acc. Chem. Res.* **2009**, *42*, 235–248.
- (10) Kaim, W.; Klein, A., Eds.; Spectroelectrochemistry; Royal Society of Chemistry: Cambridge, 2008, DOI: 10.1039/9781847558404.
- (11) Brunschwig, B. S.; Creutz, C.; Sutin, N. Optical transitions of symmetrical mixed-valence systems in the Class II—III transition regime. *Chem. Soc. Rev.* **2002**, *31*, 168–184.
- (12) Cao, Z.; Xi, B.; Jodoin, D. S.; Zhang, L.; Cummings, S. P.; Gao, Y.; Tyler, S. F.; Fanwick, P. E.; Crutchley, R. J.; Ren, T. Diruthenium-Polyyn-diyl-Diruthenium Wires: Electronic Couplings in the Long Distance Regime. *J. Am. Chem. Soc.* **2014**, *136*, 12174–12183.
- (13) Xu, G.-L.; Crutchley, R. J.; DeRosa, M. C.; Pan, Q.-J.; Zhang, H.-X.; Wang, X.; Ren, T. Strong Electronic Couplings between Ferrocenyl Centers Mediated by Bis-Ethynyl/Butadiynyl Diruthenium Bridges. *J. Am. Chem. Soc.* **2005**, *127*, 13354–13363.
- (14) Ou, Y.-P.; Zhang, J.; Zhang, M.-X.; Zhang, F.; Kuang, D.; Hartl, F.; Liu, S. H. Bonding and Electronic Properties of Linear Diethynyl Oligothienoacene-Bridged Diruthenium Complexes and Their Oxidized Forms. *Inorg. Chem.* **2017**, *56*, 11074–11086.
- (15) Zhang, J.; Zhang, M. X.; Sun, C. F.; Xu, M.; Hartl, F.; Yin, J.; Yu, G. A.; Rao, L.; Liu, S. H. Diruthenium Complexes with Bridging Diethynyl Polyaromatic Ligands: Synthesis, Spectroelectrochemistry, and Theoretical Calculations. *Organometallics* **2015**, *34*, 3967–3978.
- (16) Zhang, J.; Guo, S.-Z.; Dong, Y.-B.; Rao, L.; Yin, J.; Yu, G.-A.; Hartl, F.; Liu, S. H. Multistep Oxidation of Diethynyl Oligophenylamine-Bridged Diruthenium and Diiron Complexes. *Inorg. Chem.* **2017**, *56*, 1001–1015.
- (17) Jordan, M.; Kivala, M.; Boudon, C.; Gisselbrecht, J.-P.; Schweizer, W. B.; Seiler, P.; Diederich, F. Switching the Regioselectivity in Cycloaddition-Retro-Electrocyclizations between Donor-Activated Alkynes and the Electron-Accepting Olefins TCNE and TCNQ. *Chem. Asian J.* **2011**, *6*, 396–401.
- (18) Kivala, M.; Boudon, C.; Gisselbrecht, J. P.; Enko, B.; Seiler, P.; Muller, I. B.; Langer, N.; Jarowski, P. D.; Gescheidt, G.; Diederich, F. Organic Super-Acceptors with Efficient Intramolecular Charge-Transfer Interactions by 2+2 Cycloadditions of TCNE, TCNQ, and F-4-TCNQ to Donor-Substituted Cyanoalkynes. *Chem. Eur. J.* 2009, 15, 4111–4123.
- (19) Misra, R.; Jadhav, T.; Nevonen, D.; Monzo, E. M.; Mobin, S. M.; Nemykin, V. N. Synthesis, Structures, and Redox Properties of Tetracyano-Bridged Diferrocene Donor-Acceptor-Donor Systems. *Organometallics* **2017**, *36*, 4490–4498.
- (20) Banziger, S. D.; Ren, T. Syntheses, Structures and Bonding of 3d Metal Alkynyl Complexes of Cyclam and Its Derivatives. *J. Organomet. Chem.* **2019**, 885, 39–48.
- (21) Li, X.; Valdiviezo, J.; Banziger, S. D.; Zhang, P.; Ren, T.; Beratan, D. N.; Rubtsova, I. V. Symmetry controlled photo-selection and charge separation in butadiyne-bridged donor-bridge-acceptor compounds. *Phys. Chem. Chem. Phys.* **2020**, *22*, 9664–9676.
- (22) Banziger, S. D.; Judkins, E. C.; Zeller, M.; Ren, T. Diruthenium-DMBA Bis-Alkynyl Compounds with Hetero- and Extended-Aryl Appendant. *Chin. J. Inorg. Chem.* **2017**, 33, 2103–2109.
- (23) Gibtner, T.; Hampel, F.; Gisselbrecht, J.-P.; Hirsch, A. End-Cap Stabilized Oligoynes: Model Compounds for the Linear sp Carbon Allotrope Carbyne. *Chem. Eur. J.* **2002**, *8*, 408–432.
- (24) Krejčik, M.; Daněk, M.; Hartl, F. Simple construction of an infrared optically transparent thin-layer electrochemical cell: Applications to the redox reactions of ferrocene, Mn2(CO)10 and Mn(CO)3(3,5-di-t-butyl-catecholate). *J. Electroanal. Chem.* **1991**, 317, 179–187.
- (25) Yu, H. S.; He, X.; Li, S. L.; Truhlar, D. G. MN15: A Kohn-Sham global-hybrid exchange-correlation density functional with broad accuracy for multi-reference and single-reference systems and noncovalent interactions. *Chem. Sci.* **2016**, *7*, 5032–5051.
- (26) Weigend, F.; Ahlrichs, R. Balanced basis sets of split valence, triple zeta valence and quadruple zeta valence quality for H to Rn:

- Design and assessment of accuracy. Phys. Chem. Chem. Phys. 2005, 7, 3297-3305.
- (27) Frisch, M. J.; Trucks, G. W.; Schlegel, H. B.; Scuseria, G. E.; Robb, M. A.; Cheeseman, J. R.; Scalmani, G.; Barone, V.; Petersson, G. A.; Nakatsuji, H.et al. *Gaussian 16 Rev. B.01*; Wallingford, CT, 2016
- (28) Yanai, T.; Tew, D. P.; Handy, N. C. A new hybrid exchange-correlation functional using the Coulomb-attenuating method (CAM-B3LYP). *Chem. Phys. Lett.* **2004**, 393, 51–57.
- (29) Becke, A. D. Density-functional thermochemistry. III. The role of exact exchange. *J. Chem. Phys.* **1993**, *98*, 5648–5652.
- (30) Lee, C.; Yang, W.; Parr, R. G. Development of the Colle-Salvetti correlation-energy formula into a functional of the electron density. *Phys. Rev. B* **1988**, *37*, 785–789.
- (31) Beels, M. T.; Fleischman, M. S.; Biaggio, I.; Breiten, B.; Jordan, M.; Diederich, F. Compact TCBD based molecules and supramolecular assemblies for third-order nonlinear optics. *Opt. Mater. Express* **2012**, *2*, 294–303.
- (32) Scalmani, G.; Frisch, M. J. Continuous surface charge polarizable continuum models of solvation. I. General formalism. *J. Chem. Phys.* **2010**, 132, 114110.
- (33) Loutfy, R. O.; Loutfy, R. O. The Interrelation between Polarographic Half-wave Potentials and the Energies of Electronic Excited States. *Can. J. Chem.* 1976, 54, 1454–1463.
- (34) Banziger, S. D.; Li, X.; Valdiviezo, J.; Zeller, M.; Zhang, P.; Beratan, D. N.; Rubtsov, I.; Ren, T. Unsymmetrical Bis-Alkynyl Complexes Based on Co(III)(cyclam): Synthesis, Ultrafast Charge Separation, and Analysis. *Inorg. Chem.* **2019**, *58*, 15487–15497.
- (35) Kivala, M.; Boudon, C.; Gisselbrecht, J. P.; Seiler, P.; Gross, M.; Diederich, F. A novel reaction of 7,7,8,8-tetracyanoquinodimethane (TCNQ): charge-transfer chromophores by 2+2 cycloaddition with alkynes. *Chem. Commun.* **2007**, 4731–4733.
- (36) Betou, M.; Kerisit, N.; Meledje, E.; Leroux, Y. R.; Katan, C.; Halet, J. F.; Guillemin, J. C.; Trolez, Y. High-Yield Formation of Substituted Tetracyanobutadienes from Reaction of Ynamides with Tetracyanoethylene. *Chem. Eur. J.* **2014**, *20*, 9553–9557.
- (37) Michinobu, T.; May, J. C.; Lim, J. H.; Boudon, C.; Gisselbrecht, J.-P.; Seiler, P.; Gross, M.; Biaggio, I.; Diederich, F. A new class of organic donor—acceptor molecules with large third-order optical nonlinearities. *Chem. Commun.* **2005**, 737—739.
- (38) Shoji, T.; Miura, K.; Araki, T.; Maruyama, A.; Ohta, A.; Sekiguchi, R.; Ito, S.; Okujima, T. Synthesis of 2-Methyl-1-azulenyl Tetracyanobutadienes and Dicyanoquinodimethanes: Substituent Effect of 2-Methyl Moiety on the Azulene Ring toward the Optical and Electrochemical Properties. *J. Org. Chem.* **2018**, *83*, 6690–6705.
- (39) Yamagata, T.; Kuwabara, J.; Kanbara, T. Synthesis and Characterization of Dioxopyrrolopyrrole Derivatives Having Electron-Withdrawing Groups. *Eur. J. Org. Chem.* **2012**, 5282–5290.
- (40) Rabaâ, H.; Cundari, T. R.; Omary, M. A. Combined tight-binding/DFT investigation of the electronic structure of triimine-platinum(II)/TCNQ extended stacks 1,2. *Can. J. Chem.* **2009**, 87, 775–783
- (41) Kaim, W.; Moscherosch, M. The coordination chemistry of TCNE, TCNQ and related polynitrile π acceptors. *Coord. Chem. Rev.* **1994**, *129*, 157–193.
- (42) Peterson, J. P.; Winter, A. H. Solvent Effects on the Stability and Delocalization of Aryl Dicyanomethyl Radicals: The Captodative Effect Revisited. *J. Am. Chem. Soc.* **2019**, *141*, 12901–12906.
- (43) Khatkale, M. S.; Devlin, J. P. The vibrational and electronic spectra of the mono-, di-, and trianon salts of TCNQ. *J. Chem. Phys.* **1979**, 70, 1851–1859.
- (44) Beck, W.; Schlodder, R.; Lechler, K. H. Reaktion des radikalanions tetracyanoethylenid mit iridium(I)- und rhodium(I)-komplexen (Ph3P)2M(CO)Cl. *J. Organomet. Chem.* **1973**, *54*, 303–311.
- (45) Bureš, F.; Pytela, O.; Kivala, M.; Diederich, F. Solvatochromism as an efficient tool to study N,N-dimethylamino- and cyanosubstituted pi-conjugated molecules with an intramolecular charge-transfer absorption. *J. Phys. Org. Chem.* **2011**, *24*, 274–281.